Hindawi
Journal of Nanomaterials
Volume 2022, Article ID 1705521, 12 pages
https://doi.org/10.1155/2022/1705521

*Research Article*

# High-Efficiency Power Generation Device of Magnetic Declination Thermoelectric Material and Multisource Coordination Optimization of Distribution Network

**Lifeng Zhang and Xiaofang Wu**

*Ordos Vocational College, Ordos, 017000 Ordos, China*

Correspondence should be addressed to Xiaofang Wu; zlf1115@imut.edu.cn

Received 23 March 2022; Revised 28 April 2022; Accepted 11 May 2022; Published 1 June 2022

Academic Editor: Awais Ahmed



The first-order phase transition compounds have attracted widespread attention from refrigeration enterprises and scientists due to their giant magnetocaloric effect and refrigeration temperature region spanning room temperature. Magnetic substances are crystal structures composed of magnetic ions or atoms with a certain thermal motion or vibration. This research mainly discusses the multisource coordination optimization of magnetic declination thermoelectric material efficient power generation device and distribution network. In this study, large doses of MnFe(P,Si) compounds with different ratios were prepared. The reason for choosing a large dose is that the properties and structures of the samples prepared in a large amount and a small amount will be more or less the same for the samples fired in the same proportion and in the same process. At the same time, mass production also prepares for future mass production. Thermomagnetic power generation described in this study is a form of power generation that converts thermal energy directly into electrical energy. The conversion of thermal energy to electric energy is realized by the change of magnetization in the closed coil by the thermomagnetic material in the magnetic field environment, and then, the change of the magnetic flux in the closed coil is realized. The distribution network refers to the power network that receives electrical energy from the transmission network or regional power plants and distributes it locally through distribution facilities or distributes it to various users step by step according to the voltage. It is composed of overhead lines, cables, towers, distribution transformers, isolating switches, reactive power compensators, and some ancillary facilities. A network that plays an important role in distributing electrical energy in the power grid. This research starts with the active distribution network scheduling priority and the distribution network scheduling coordination control framework. Combined with the scheduling and operation characteristics of each component in the distribution network, the coordinated optimization scheme of the distribution network and the source-network load-storage coordinated control framework are investigated and analyzed. The scheduling resources of the model include the power of the substation flowing into the distribution network, the output of the adjustable distributed power source, the output value of the energy storage element, the closing status of the tie switch, and the section switch. In the study, it was found that when the Fe content was 0.63, the Curie temperature of the compound could reach 273 K at the highest. Scientifically designing a thermomagnetic power generation demonstration device is an important part of the realization of thermomagnetic power generation. The magnetic declination thermoelectric materials designed in this study will help to improve the power generation efficiency.

## 1. Introduction

The rapid development of nanotechnology and advanced material synthesis technology provides convenience for the continuous improvement of the dimensionless thermoelectric figure of merit of thermoelectric materials. This in turn promotes thermoelectric power generation technology to play an active role in civil fields, such as automobiles and ships. Thermoelectric power generation technology has both social and economic benefits in the recycling and reuse of industrial waste energy.

Although the power generation efficiency of the energy system is reduced when the scale is reduced, its consequent reduction in transmission losses makes people see the feasibility of studying such systems. As a new microminiature energy source, the microthermoelectric power generation system has no moving parts, reliable operation, no noise, and low pollution. It can be an ideal solution as a miniature power supply for electronic systems. Compared with traditional energy, new energy has many advantages, but due to various technical defects, there is no new energy that can replace the dominant position of fossil energy in the energy structure.

It gives the temperature distribution function in the magnetic declination thermoelectric system structure according to the energy relation. It also uses the existing thermoelectric module parameters to establish continuous mathematical models for the one-dimensional symmetric and two-dimensional symmetric thermoelectric system structures. It also gives a discrete mathematical model for the distribution law of thermocouple pairs. On this basis, necessary parameter corrections were made to the model in combination with factors such as heat conduction process, structural gap, energy dissipation, and the adoption of porous structure. Thermocouples are temperature measuring elements commonly used in temperature measuring instruments. It is based on making full use of the continuity of the temperature distribution function of the system and discretizing the thermocouple pair. It performs multivariate optimization on the parameters of the thermoelectric system structure model. Based on the design goals, this paper proposes design indicators such as system efficiency function and volume energy density function and obtains the optimal value range of the system structure size and main model parameters.

## 2. Related Work

As a new microminiature energy source, the magnetic declination thermoelectric power generation system has no moving parts, no noise, reliable operation, and low pollution. It can be used as an ideal solution for the micropower supply of electronic systems. Magnetic declination refers to the angle between the magnetic meridian at any point on the earth's surface and the geographic meridian. Because compass and magnetic compass are the simplest devices to measure magnetic declination, the history of discovery and measurement of magnetic declination is also very early. Takahashi et al. believed that the power package dispatch system is expected to become one of the advanced distribution systems for controlling power, providing energy on demand, and reducing energy consumption. They designed and experimentally verified a power packet router to implement a networked power packet distribution system. Previously developed routers forwarded power packets directly to the load. And the new router forwards the packet to the other router with an information tag reattached to the power payload. In addition, new routers can adjust the start time of forwarding received power packets to other sites, thereby taking advantage of the router's integrated storage capacity [1]. Wang and Lin studied the Minimum Distribution Cost Problem (MDCP) for a flow model of specialized manufacturing networks in order to simulate the distillation or decomposition of products in some manufacturing processes [2]. Ravadanegh et al. developed an integrated approach to the problem consisting of power distribution system reconfiguration, capacitor allocation, and simultaneous sizing and siting of renewable energy sources. It also improves the accountability and system performance parameters of the power system. They looked for solutions that are closer to the characteristics of reality. Load forecasts, market price errors, and uncertainties associated with variable output power of wind-distributed generators were all taken into account. They adopted NSGA-II combined with fuzzy set theory to solve the above multiobjective problem. The scheme they proposed ultimately resulted in a solution with minimum voltage deviation, maximum voltage stability, less contamination, and lower cost. Costs include new equipment installation cost, reconfiguration cost, power loss cost, reliability cost, cost of purchasing energy from the electricity market, line upgrade cost, and operation and maintenance cost of distributed generation [3]. Mehmood et al. believed that the life of a battery in a battery energy storage system (BESS) is affected by various factors such as the battery's operating temperature, depth of discharge, and the amount of charge/discharge current supplied to or drawn from the battery. They found the optimal location and size of the BESS for voltage regulation in power distribution systems [4]. Kulmala et al. believed that congestion management is one of the core drivers of smart power distribution systems. Distributed energy sources were used for network control for cost-effective network interconnection of distributed generation (DG) and better utilization of network assets. The main purpose of congestion management was to prevent voltage violations and overload the network. Congestion management algorithms can also be used to optimize network status. They proposed hierarchical and distributed congestion management concepts for future distribution networks with large-scale DG and other controllable resources in medium- and low-voltage networks. The control concept aims to run the network at the lowest cost while maintaining an acceptable network state. The hierarchy consists of three levels: the primary controller operates based on local measurements, the secondary control optimizes the set point of the primary controller in real-time, and the tertiary control utilizes load and production forecasts as its inputs. It implements network reconstruction algorithms and connections to the market. The primary controller is at the connection point of the controllable resource. The secondary controller is located in the primary and secondary substations, and the tertiary control is located in the control center. Therefore, the control is spatially distributed and operates on different time scales [5]. Mohtashami et al. proposed a multiyear distribution network planning optimization model. This was used to manage the operations and capacity of distribution systems with significant penetration of distributed generation (DG). Models take into account investments in traditional network and smart grid technologies. It includes dynamic line ratings, quadrature boosters, and

active network management. It also optimizes the settings of network control devices and takes into account their network cut DG output access arrangements (corporate or noncorporate) when necessary. They had carried out a series of studies on the UK 33 kV actual distribution network to test the model. The main purpose of the research was to evaluate and compare the performance of different investment methods, namely, incremental investment and strategic investment. The study also demonstrated the ability of the model to determine the optimal DG connection point to reduce the overall system cost [6]. Chen et al. through Matlab modeling and simulation proved that the algorithm was suitable for distributed generation (DG) distribution network fault location, which has a certain rapidity and fault tolerance [7]. The introduction of new energy will bring new problems and inconveniences in energy conversion, management, operation, etc., which requires the study of new supporting technologies for coordination. With the development of society, the depletion of fossil energy and the indiscriminate exploitation of resources has led to environmental deterioration, and the situation faced by human beings has become more and more severe. Under the current situation, many countries are vigorously developing green energy and have made considerable achievements. The introduction of new energy will bring new problems and inconveniences in energy conversion, management, operation, etc., which require the study of new supporting technologies for coordination. Therefore, how to comprehensively utilize new energy and traditional energy and realize the complementary advantages between the two is an important issue we are currently facing. As a developing country, China is developing rapidly, and energy consumption and heat emission are topics that cannot be underestimated. A large amount of heat energy emissions will not only bring environmental problems but also aggravate natural disasters such as the greenhouse effect and acid rain.

## 3. Methods for High-Efficiency Power Generation of Magnetic Declination Thermoelectric Materials

*3.1. Thermoelectric Materials for Power Generation.* Assuming that the internal load of a thermoelectric material module is $R_L$, a heat source $q$ can also be added to provide heat so that the temperature difference between the two ends of the conductor is maintained by $T_1 - T_2$. The potential difference generated across the conductor is $(S_2 - S_1) * (S_1 - S_2)$, and the power generated is [8]

$$W = \left[\frac{(\beta_P - \beta_N)(T_1 - T_2)}{R_L - R}\right]^2 R_L. \tag{1}$$

Considering the heat flow provided by the heat source, most of the heat passes through the conductors by means of heat conduction. But there are parts of the heat flow that need to be balanced against the Peltier effect and Joule heating in general. The Peltier effect means that when a current passes through a loop composed of different conductors, in addition to irreversible Joule heat, the junctions of different conductors will endothermic and exothermic phenomena with different current directions.

$$Q = k(T_1 - T_2) + (\beta_1 - \beta_2)IT_1 - \frac{I^2R}{2}. \tag{2}$$

The current density $I$ is

$$I = \frac{(\beta_1 - \beta_2)(T_1 - T_2)}{(R_1 + R_2)}. \tag{3}$$

Therefore, the choice of load is generally to achieve maximum efficiency [9]

$$M = (1 + ZT)^{1/2}. \tag{4}$$

It gets the efficiency formula:

$$\eta = \frac{T_1 - T_2}{T_1} \cdot \frac{M - 1}{M + \chi T_1/T_2}. \tag{5}$$

It can be seen that the larger the $M$, the higher the efficiency. However, the size of $M$ is mainly related to $Z$ and temperature, so the value of $ZT$ has a great influence on the efficiency of TEG materials.

For the design of thermoelectric sheets and the modeling of microminiature thermal structures, this paper is aimed at designing a microminiature thermoelectric conversion system as efficient as possible. Thermoelectric conversion systems are usually composed of thermal structures and thermoelectric conversion modules. Therefore, a thermoelectric unit model that comprehensively considers the thermal model and the electrical model is established. After that, it will build a complete thermoelectric conversion system model on this basis. The materials used to manufacture thermoelectric generators or thermoelectric coolers are called thermoelectric materials, which are materials that can realize the interactive transformation of electrical energy and thermal energy.

*3.2. Principle of Thermomagnetic Power Generation Device.* When the thermomagnetic power generation material (Mn, Fe)2(P, Si) is in a strong magnetic field, when the hot water passes through, when the temperature is higher than the Curie temperature of the thermomagnetic power generation material, the thermal motion of the atoms intensifies. The kinetic energy possessed by the thermal motion of atoms is sufficient to overcome the exchange between spin-magnetic moments. The spin moment of the magnetic atoms inside the material changes from parallel arrangement to disorder, and the magnetization becomes zero instantaneously. The thermomagnetic power generation material is transformed from a ferromagnetic state to a paramagnetic state, and the magnetic field becomes smaller. When the magnetic flux passing through the induction coil decreases, an induced current is generated in the induction coil. Conversely, when cold water passes through, the temperature of the thermomagnetic power generation material is lower than the Curie

temperature, and the atomic thermal motion weakens when the temperature decreases. The exchange action between the spin magnetic moments makes the magnetic atom spin magnetic moments return to the parallel arrangement from the disorderly arrangement. The magnetization changes from zero to a certain value instantaneously, and the thermomagnetic power generation material changes from a paramagnetic state to a ferromagnetic state. When the magnetic field increases, the magnetic flux passing through the induction coil increases, which will also generate a reverse induced current in the induction coil. Hot water and cold water alternately pass through the induction coil plastic tube thermomagnetic power generation material, and the ferromagnetic state and paramagnetic state of the thermomagnetic power generation material periodically transform each other near the Curie temperature. This will generate a periodic alternating induced current and realize the direct conversion of thermal energy into electrical energy. The principle of thermomagnetic power generation device is shown in Figure 1. For the design of thermoelectric power generation sheet, it is generally required that the larger the output power per unit volume, the better, that is, the larger the volume-specific power, the better. In the actual design process, when the area and other parameters of the thermoelectric power generation sheet are determined, and the length of the galvanic coupler arm is short to a certain extent; the output power of the power generation sheet will reach the maximum. If it continues to shorten, its power will show a downward trend [10].

For the energy storage devices connected in the network, the property rights are set to be owned by the distribution network operation and maintenance company, and they can participate in the operation and scheduling of the distribution network. Its scheduling cost $C_t^E$:

$$C_t^E = \sum \lambda P_t^E \Delta T \tag{6}$$

For any distribution network node $i$, the power balance formula in polar coordinate form can be listed as follows [11]

$$P_i = U \sum U(G \cos \beta + B \sin \beta) \tag{7}$$

$$Q_i = U \sum U(G \cos \beta - B \sin \beta) \tag{8}$$

Among them: $P_i$ and $Q_i$ are the injected active and reactive power of node $i$, respectively [12].

When using Newton-Raphson's method to solve a nonlinear system of equations, it is necessary to write out its modified equations [13]

$$\Delta P_i = P - U_i \sum U(G \cos \beta + B \sin \beta), \tag{9}$$

$$\Delta Q_i = P - U_i \sum U(G \cos \beta - B \sin \beta). \tag{10}$$

### 3.3. $Mn_{1.23}FexP_{0.3}Si_{0.3}$ Compound Structure and Magnetic Test

*3.3.1. Material Preparation.* The Mn flakes, Fe powder, P powder, and single-crystal Si block used in the experiment are calculated in a ratio of $Mn_{1.23}Fe_xP_{0.3}Si_{0.3}$ ($x = 0.6$, 0.63, 0.63, 0.67, 0.7, and 0.73). It is weighed with an electronic balance. It was ball milled with a high-energy planetary ball mill (pulverisette-3) for 10 h under argon protection. It then precompresses the sample into a block under the pressure of 8 T and then puts it into a quartz tube for vacuuming (vacuum degree < 10-3 Pa), fills it with argon gas to $2 \times 103$ Pa, and seals the quartz tube. The sealed samples were placed in a vertical annealing furnace for sintering at 11009°C for 2 h and then lowered to 830°C for 20 h and then quenched.

*3.3.2. Sample Characterization and Performance Measurement.* The X-ray diffraction (XRD) spectrum of the sample was measured with a Philips PW-1830 X-ray diffractometer (Cu-K$\alpha$, $h = 0.134184$ nm) at room temperature (293 K), the measurement step was 0.01°, and the collection point time was 4 s. It measures the magnetic properties of compounds with a LakeShore 7407 vibrating sample magnetometer [14].

Voltage constraints:

$$V_{K,\min} < V_K < V_{K,\max}, \tag{11}$$

where $V_k$ is the voltage at node $k$ [15].

Line current constraints:

$$I \le I_{l,\max}, \quad l \in n_l. \tag{12}$$

In the formula, $I_l$ is the number of branches in the power supply island network after the power supply is restored. $I_{l,\max}$ is the maximum current value allowed for line $I$.

Microgrid output constraints [16]

$$P_{j,\min} \le P \le P_{j,\max}. \tag{13}$$

$P_{j,\max}$ and $P_{j,\min}$ are the upper and lower limits of the active power sent by the microgrid $j$, respectively [17].

Charge load available capacity constraints [18]

$$EV \le EV_{k,\max}. \tag{14}$$

$EV_{k,\max}$ is the upper limit of the available capacity of the charging power [19].

The dispatch model takes the total operating cost of the distribution network in a single dispatch period as the objective function.

$$\min F = \sum \left(C_t^g + C_t^{\mathrm{DG}} + C_t^{\mathrm{ESS}} + C_D^t\right). \tag{15}$$

In the formula, time $t$ represents the current time period [20].

The cost of purchasing electricity from the grid:

$$C_b = \sum_g^{NG} CP\Delta T. \tag{16}$$

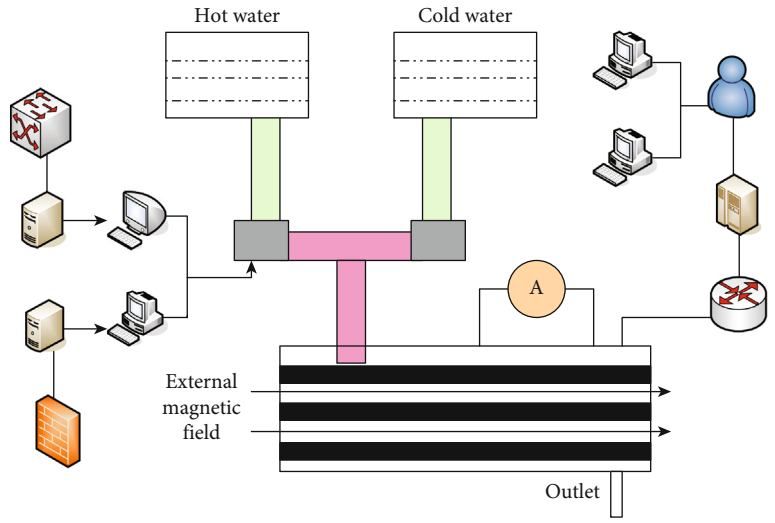


Figure 1: Principle of thermomagnetic power generation device.

Among them, $g$ represents the feeder at the exit of the $b$ substation, and NG represents the total number of substation feeders connected to the distribution network.

*3.4. Design of Thermomagnetic Power Generation Device.* The thermomagnetic power generation device is composed of six parts: magnetic field system, cold and heat source system, automatic control electronic switch, induction coil, sensitive ammeter, and thermomagnetic power generation material.

(1) Magnetic field system: the strong magnetic material NdFeB is used to make a cylindrical strong permanent magnet as the driving magnetic field. The length is 20 cm, the inner diameter is 9 cm, the outer diameter is 20 cm, and the maximum magnetic induction intensity is $B = 0.8$ T. The direction of the magnetic field is radial. The plastic tube with the magnetic material placed in the outer coil is placed in the inner magnetic field area of the cylindrical strong magnet, and its function is to make the thermomagnetic power generation material reach saturation magnetization

(2) Cold and heat source system: the heat source is a domestic water heater, the maximum temperature can reach 100°C; the cold source is tap water

(3) Automatic electronic switch: the two electronic switches are, respectively, connected with the heat source and the cold source water inlet pipe. The electronic switch is controlled by a single-chip microcomputer. The hot and cold water passes through the thermomagnetic power generation material in the plastic pipe alternately, and different times can be set according to needs. The thermomagnetic power generation material periodically changes in cold and heat

(4) Induction coil: the induction coil is wound on a plastic tube by a hand-winding machine, and the wound coil is painted with insulating paint to protect the coil. After the thermal-magnetic power generation material is installed inside the plastic pipe, the two ends are cut with nylon rods and the outside is sealed with a rubber sheet

(5) Microammeter: measure the thermal-magnetic power generation current, and use wires to connect the induction coil and the microammeter [21]

(6) Thermomagnetic power generation material: the annealed thermomagnetic power generation material is cut into 1.3 mm thin slices with a wire cutting machine. The thin copper wires are used to connect them, leaving a gap in the middle to facilitate the passage of water and improve the heat exchange capacity between the material and water. The cut thermomagnetic power generation material can also be turned into small particles. The thermomagnetic power generation device designed in this study is shown in Figure 2

*3.5. Multisource Optimization Model for Microgrid Power Supply Recovery.* After the distribution network fails, the real-time monitoring of the DMS is used to obtain the sum of the power available for all microgrids in the outage area $\sum L_i$ and the total power $\sum MG_j$ of the load in the outage area, and the microgrid power supply recovery scheme is selected [22].

$$\sum L_i \le \sum MG_j. \tag{17}$$

After the power distribution network fails, the real-time monitoring of DMS is used to obtain the sum of the external power of all microgrids in the nonfault outage area $\sum MG$

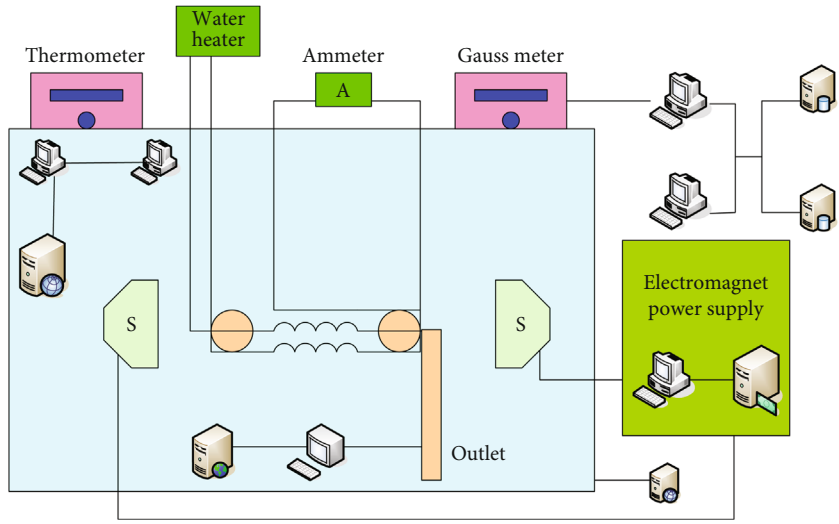


Figure 2: The thermomagnetic power generation device designed in this paper.

and the total power of the load in the outage area $\sum L_i$.

$$\sum L - \sum EV \le \sum MG \le \sum L_i. \tag{18}$$

The multilevel rapid power supply restoration scheme proposed in this study considers the economics of network operation after the power supply of the distribution network is restored. Therefore, in the optimal power flow mathematical model, the optimization objective is to minimize the active network loss of the power supply island after the power supply is restored [23]

$$\min M = \min \sum I^2 R, \tag{19}$$

where $I$ is the line transmission current; $R$ is the line resistance.

The theoretical output power of a single thermocouple pair tends to increase with the increase of the temperature difference between its two sides in a large range and also tends to increase with the increase of the current. In comparison, the effect of temperature difference on the thermocouple's power generation efficiency is more obvious. Tide constraints:

$$U \sum_{J=1} YU = P + Q, \tag{20}$$

where $P$ and $Q$ are the values of active power and reactive power injected by node $i$, respectively.

## 4. Multisource Coordination Optimization Results of Thermoelectric Material Efficient Power Generation Device and Distribution Network

Figure 3 shows the XRD spectrum of the $Mn_{1.23}FexP_{0.3}Si_{0.3}$ series compounds. It can be seen from the XRD spectrum that when the Fe content is 0.63, it is a single $Fe_2P$-type hexagonal structure. The impurity phase of this series of compounds is one of $(Mn, Fe)_3Si$ or $(Mn, Fe)_3Si_3$. With the increase of Fe content, the first impurity phase is $(Mn, Fe)_3Si_3$. Then, the peak intensity decreased gradually until the Fe content was 0.67, the $(Mn, Fe)_3Si$ impurity phase appeared, and then the peak intensity gradually increased.

It can be seen from Table 1 that when $x$ is between 0.6 and 0.63, the unit cell volume $V$ and the lattice constant $a$ gradually increase. When $x$ is between 0.63 and 0.73, the change rule of the unit cell volume $V$ is not obvious. The lattice constants and unit cell volumes of the $Mn_{1.23}FexP_{0.3}Si_{0.3}$ series compounds are shown in Table 1.

The change of magnetization with temperature of $Mn_{1.23}FexP_{0.3}Si_{0.3}$ ($x = 0.6$, 0.63, 0.63, 0.67, 0.7, and 0.73) series compounds is shown in Figure 4. The cooling and heating curves do not overlap, indicating that there is thermal hysteresis. When the Fe content is 0.63, the thermal hysteresis of the compound is at least 1 K. When the Fe content is 0.6, the maximum thermal hysteresis of the compound is 21 K. The Curie temperature (Tc) of a compound can be determined by taking the partial derivative of the M-T heating curve. It can be seen that when the Fe content is 0.63, the maximum Curie temperature of the compound is 273 K. When the Fe content is 0.6, the minimum Curie temperature of the compound is 207 K.

$Mn_{1.23}FexP_{0.3}Si_{0.3}$ samples were prepared and cut into 1.3 mm thin slices by a wire cutting machine. The samples were taken with masses of 30 g, 100 g, 130 g, and 200 g, respectively, and put into a thermomagnetic power generation device with $N = 1030$, 2000, 2700, and 3300 coil turns, and the hot water temperature was about 80°C. Through the analysis of the measurement data, whether it is a flake sample or a particle sample, the induced current increases with the increase of the sample mass. The reason is that the mass increases, the total number of magnetic atoms increases, the total magnetic moment increases, and the change rate of the total magnetic flux of the sample around the Curie temperature increases. For samples of the same mass, the induced current produced by the granular sample

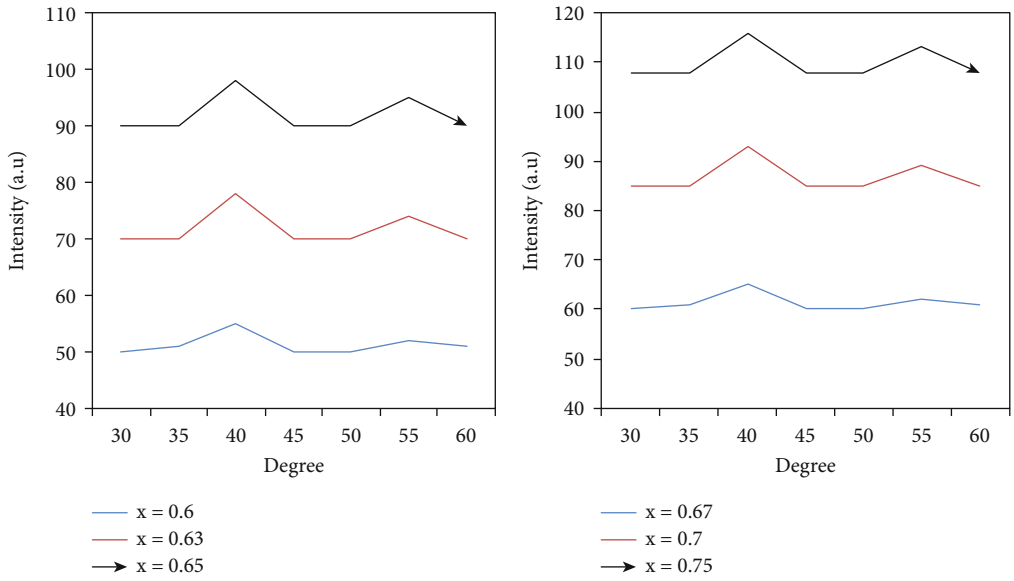


Figure 3: XRD spectra of $Mn_{1.23}Fe_xP_{0.3}Si_{0.3}$ series compounds.

Table 1: Lattice constant and unit cell volume of $Mn_{1.23}Fe_xP_{0.3}Si_{0.3}$ series compounds.

| $x$ | $a$ (nm) | $c$ (nm) | $V$ ($nm^3$) |
|---|---|---|---|
| 0.6 | 0.6030 | 0.3414 | 0.1082 |
| 0.63 | 0.6064 | 0.3399 | 0.1083 |
| 0.63 | 0.6063 | 0.3404 | 0.1083 |
| 0.67 | 0.6060 | 0.3407 | 0.1084 |
| 0.7 | 0.6048 | 0.3407 | 0.1079 |
| 0.73 | 0.6012 | 0.3480 | 0.1089 |

is greater than that produced by the flake sample. The variation of the induced current is shown in Figure 5.

When a sample of the same mass is placed in the coil, the induced current $I$ increases with the increase of the number of turns $N$ of the coil. According to Faraday's law of electromagnetic induction, the induced electromotive force is proportional to the number of turns of the coil. The relationship between the induced current and the number of coil turns is shown in Figure 6.

Figure 7 shows the XRD diffraction of Sn-bonded $Mn_{1.23}Fe_{0.63}P_{0.3} - xSi_{0.3} + x$ series composite compounds. Through qualitative analysis of XRD patterns, it can be known that the compound and the main phase are still $Fe_2P$-type structure of MnFe(P,Si).

This shows that the main phase structure of the bonded compound has not changed (A ($Mn_{1.23}Fe_{0.63}P_{0.48}Si_{0.32}$), B ($Mn_{1.23}Fe_{0.63}P_{0.46}Si_{0.34}$), C ($Mn_{1.23}Fe_{0.63}P_{0.44}Si_{0.36}$), and D ($Mn_{1.23}Fe_{0.63}P_{0.42}Si_{0.38}$)). There is an impurity peak around 43° which is $Fe_3Si_3$. After data comparison, it is found that the peaks at 31.7° and 32.3° belong to metal Sn. Both metallic Sn and impurity peaks have negative effects on the magnetocaloric properties of the compounds themselves.

The lattice constants and unit cell volumes of the $Mn_{1.23}Fe_{0.63}P_{0.3} - xSi_{0.3} + x$ series bonding compounds are shown in Table 2. From Table 2, we can see that the lattice constants $a$ and $b$ and the unit cell volume $V$ have no significant changes. It can only be seen that the lattice constant $a$ slowly decreases, $b$ increases slowly, and the unit cell volume $V$ gradually increases. The lattice constants and unit cell volumes of the $Mn_{1.23}Fe_{0.63}P_{0.3} - xSi_{0.3} + x$ series bonding compounds are shown in Table 2.

The output results of the nonlinear active distribution network multisource collaborative optimization scheduling model are shown in Table 3.

Because this model is linear, the linear programming solver CPLEX is used to solve it. The calculation time is 2.9 s, and the total running cost is 27728.922 yuan. It can be seen that the fast calculation method can greatly improve the solution speed while maintaining high accuracy. The improvement of computational efficiency brought by the linear algorithm is more obvious in solving large-scale systems with multiple nodes and multiple times. The planned output power of the substation within 24 hours is shown in Figure 8.

Based on the multisource collaborative optimization nonlinear scheduling model of network reconfiguration, the SBB mixed integer nonlinear programming solver is called in GAMS, and the optimal collaborative scheduling scheme of active distribution network energy storage, flexible load, and tie switch position control is obtained. Compared with the operation results obtained by the dispatching model without considering dynamic reconfiguration, it can verify the effective application of dynamic reconfiguration in the coordinated optimal operation of the distribution network system. The planned output of the substation is shown in Table 4.

Strategy 2 considers energy storage factors more than strategy 1. The total operating cost of the active distribution network is reduced by 3383.42 yuan, and the electricity sales revenue from the distribution network to the main network

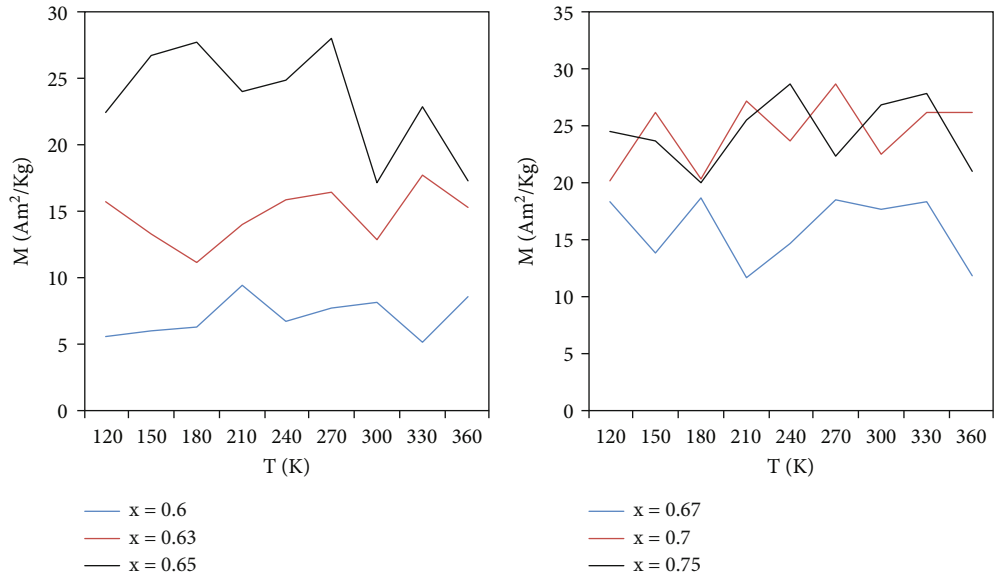


Figure 4: Magnetization of $Mn_{1.23}FexP_{0.3}Si_{0.3}$ ($x = 0.6$, 0.63, 0.63, 0.67, 0.7, and 0.73) series compounds as a function of temperature.

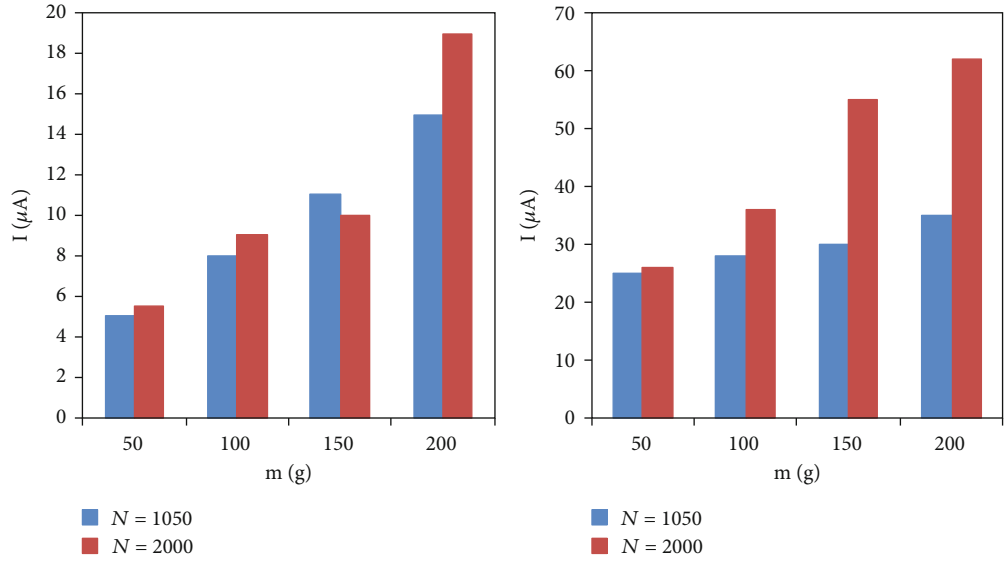


Figure 5: Variation of induced current.

is 996.03 yuan, an increase of 734.13 yuan compared with strategy 1. The operating costs of the distribution network under different dispatching strategies are shown in Table 5.

The operator's distributed power parameters are shown in Table 6.

The matching and optimization process of each parameter inside the thermoelectric power generation device is an extremely comprehensive problem. It is not only related to material technology but also related to factors such as structure selection and layout. Therefore, another important research direction to improve the system thermoelectric power generation efficiency is to balance the influence of various parameters on the output power and thermoelectric conversion efficiency to seek the optimal matching. The load state of the active distribution network is shown in Figure 9.

## 5. Discussion

In the past few hundred years, with the rapid development of industrialization and urbanization all over the world, the demand for energy has also increased rapidly. The excavation and utilization of large-scale fossil energy have resulted in a sharp decrease in energy reserves, and at the same time, the harmful substances produced during energy consumption also directly lead to the deterioration of the environment. At this stage, adjusting the energy structure transformation is an effective way to solve the current global energy and environmental problems.

The access of distributed power sources changes the power flow direction and network structure of the distribution network. When its penetration rate is too high, it may

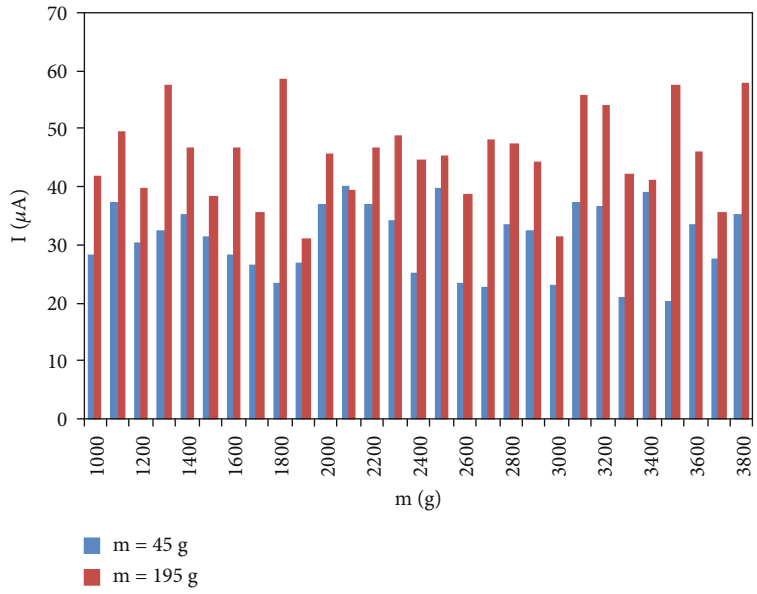


Figure 6: Induced current vs. coil turns.

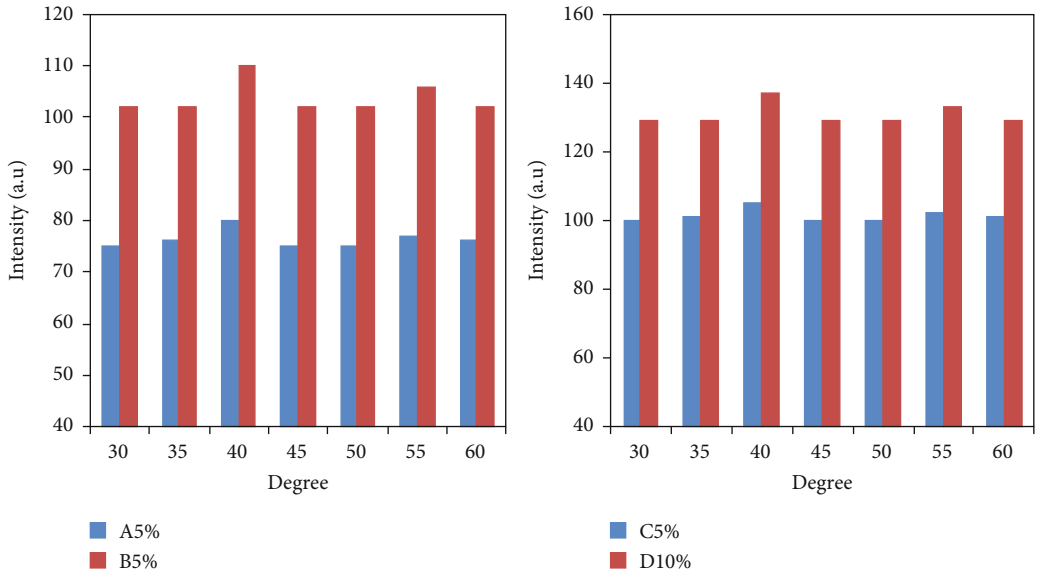


Figure 7: XRD diffraction of Sn-bonded $Mn_{1.23}Fe_{0.63}P_{0.3} - xSi_{0.3} + x$ series composite compounds.

Table 2: Lattice constant and unit cell volume of $Mn_{1.23}Fe_{0.63}P_{0.3} - xSi_{0.3} + x$ series bonding compounds.

| Serial number | $a$ (nm) | $c$ (nm) | $V$ (nm$^3$) |
|---|---|---|---|
| 3%A&B | 2.6272 | 2.3313 | 2.1281 |
| 10%A&B | 2.6263 | 2.3399 | 2.1283 |
| 3%C&D | 2.6267 | 2.3323 | 2.1287 |
| 10%C&D | 2.6262 | 2.3327 | 2.1 283 |

Table 3: Output results of multisource collaborative optimization scheduling model using nonlinear active distribution network.

| Active P (MW) | Period |
|---|---|
| T1 | 2.6307 |
| T2 | 2.7338 |
| T3 | 2.1798 |
| T4 | 2.2633 |
| T5 | 2.6834 |

cause the voltage limit of multiple distribution network nodes mainly access nodes to be exceeded, and the power flow will be sent back to the upper-level power grid. In addition, the randomness and intermittency of the distributed power supply itself will also cause problems such as voltage fluctuations in the distribution network. In the military, the use of a microthermoelectric power generation system can greatly improve the combat effectiveness of the army. Microthermoelectric power generation systems can provide

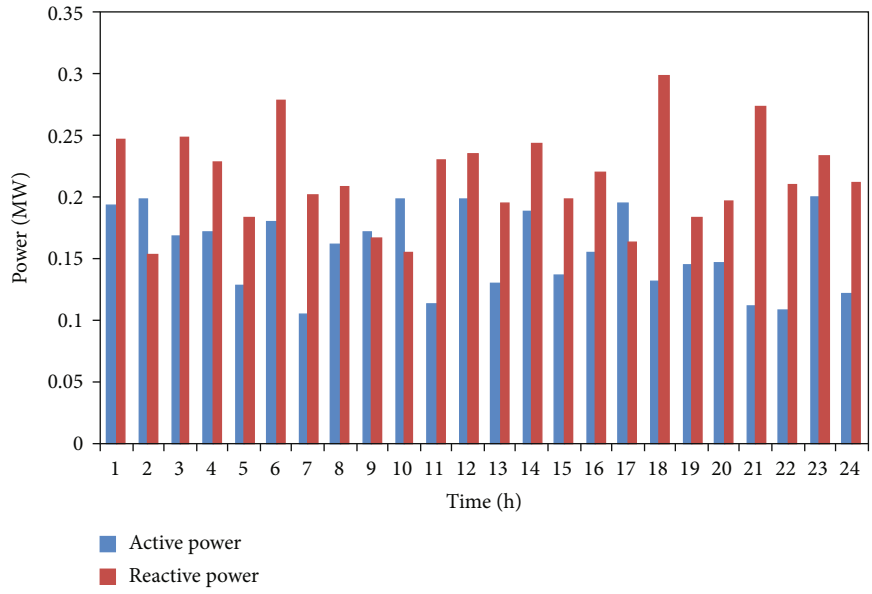


Figure 8: Substation planned output power within 24 h.

Table 4: Substation planned output.

| Time | Substation (MW) | |
|---|---|---|
| | First | Second |
| T1 | 4.2 | 0.8 |
| T2 | 3.3 | 1.7 |
| T3 | 3.1 | 2.3 |
| T5 | 2.6 | 3.4 |
| T6 | 2.1 | 4.2 |

Table 5: Distribution network operating costs under different dispatch strategies.

| Strategy | Power generation cost (yuan) | Equivalent operating cost of energy storage (yuan) |
|---|---|---|
| Strategy 1 | 24747.7 | 4272 |
| Strategy 2 | 16949.2 | 4272.4 |
| Strategy 3 | 17476.4 | 4272 |
| Strategy 4 | 22742.3 | 4212.4 |
| Strategy 5 | 14421.2 | 2177.4 |

power drives for military robots or military electronic equipment. When military robots are used for reconnaissance, their volume is generally relatively small due to the need for concealment. In field operations, the conventional power system has been unable to ensure the smooth flow of military communications, which requires the miniaturization of the power system. In these cases, energy supply is very important. In addition to the characteristics of large volume,

Table 6: Distributed power parameters for operators.

| Distributed power | Installed capacity (kW) | Number of installed units (units) |
|---|---|---|
| Photovoltaic | 350 | 10 |
| Diesel generators | 350 | 6 |
| Micro gas turbine | 520 | 2 |
| Energy storage device | 610 | 2 |

the biggest weakness of the existing technology, storage battery, fuel cell, etc., is that the time that can provide electric energy is short. The microthermoelectric power generation system can provide a relatively long power supply in a small volume.

Distributed power generation is an important way to utilize new energy. With the advancement of energy transformation and the increase of energy demand, the penetration rate of distributed power generation in the distribution network is gradually increasing. The large-scale access of DG has changed the structure of the original distribution network. Coupled with the uncertainty of DG's own output, when it is connected to different capacities and different locations, it will have different effects on the operating characteristics of the distribution network such as voltage distribution. Combined with the distribution law of the temperature field and its potential field, comprehensively considering the output characteristics and structural reliability of thermoelectric power generation, the parameters of the thermoelectric power generation device are optimized and matched, and a reasonable structural layout scheme is designed. It improves the thermoelectric conversion efficiency while reducing reliability problems caused by mechanical stress and environmental factors.

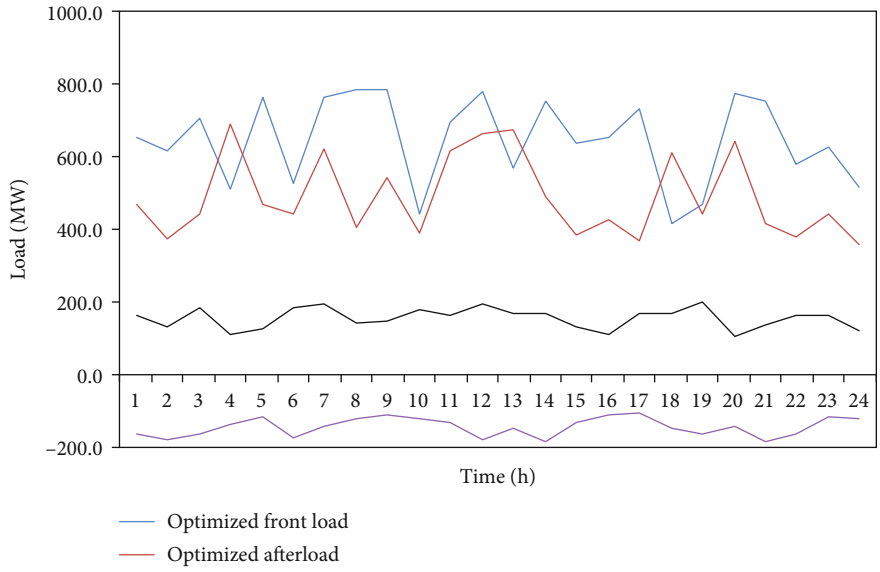


Figure 9: Load status of active distribution network.

In addition to increasing the temperature of the heat source, improving the heat dissipation conditions of the cold source and rationally arranging the cooling system are also effective ways to improve the thermoelectric conversion efficiency of the system and improve the performance of the system. First of all, choosing a reasonable heat exchange method and heat exchange medium, such as oil cooling, air cooling, water cooling, or phase change heat, can improve the performance of the system to a certain extent. Secondly, optimizing the shape and structure of the radiator components and increasing the heat dissipation area of the radiator components are important measures to improve and maintain the system temperature difference.

The characteristics of thermoelectric power generation devices make such devices play a more important role in plateau weather stations, outposts, and other places where electricity is difficult to use. When natural gas or oil pipelines pass through desolate areas, the combustion heat of natural gas or oil can be used to provide them with a temperature difference working environment. The performance of magnetic declination thermoelectric materials is also related to temperature difference. This means that both the thermal conductivity and the electrical conductivity of the material will affect the thermoelectric conversion efficiency of the material.

## 6. Conclusion

The thermal conductivity and electrical conductivity of magnetic declination thermoelectric materials are realized by the movement of internal carriers. Metal Sn and metal Zn are light metals with low melting point and good electrical conductivity. The powder compound of metal Zn or metal Sn and MnFe(P, Si) material is mixed uniformly, sealed in a quartz tube under the protection of high-purity argon gas, and sintered near the melting point of metal Zn or metal Sn. This makes the metal Sn or the metal Zn dissolve rapidly to function as a metal bond. The efficiency of the thermoelectric power generation device also depends on the heat dissipation and heat conduction device matched with it, as well as the thermoelectric coupling effect inside the thermoelectric power generation device. Therefore, the efficiency of thermoelectric conversion device is also related to parameters such as temperature difference, load resistance, loop current, and internal resistance of power generation devices. Therefore, the optimal matching between the load and the internal structural parameters of the thermoelectric power generation device is also an important issue to improve the thermoelectric conversion efficiency of the system.

## Data Availability

No data were used to support this study.

## Conflicts of Interest

There are no potential competing interests in our paper.

## Authors' Contributions

All authors have seen the manuscript and approved to submit it to your journal.

## Acknowledgments

This work was supported by the Research Program of Science and Technology at Universities of Inner Mongolia Autonomous Region (NJZY19319 and NJZY20218).

## References

[1] R. Takahashi, K. Tashiro, and T. Hikihara, "Router for power packet distribution network: design and experimental verification," *IEEE Transactions on Smart Grid*, vol. 6, no. 2, pp. 618–626, 2015.

[2] I. L. Wang and S. J. Lin, "A network simplex algorithm for solving the minimum distribution cost problem," *Journal of Industrial & Management Optimization*, vol. 3, no. 4, pp. 929-930, 2017.

[3] S. N. Ravadanegh, M. Oskuee, and M. Karimi, "Multi-objective planning model for simultaneous reconfiguration of power distribution network and allocation of renewable energy resources and capacitors with considering uncertainties," *Journal of Central South University*, vol. 24, no. 8, pp. 1837–1849, 2017.

[4] K. K. Mehmood, S. U. Khan, and S. J. Lee, "Optimal sizing and allocation of battery energy storage systems with wind and solar power DGs in a distribution network for voltage regulation considering the lifespan of batteries," *IET Renewable Power Generation*, vol. 11, no. 10, pp. 1303–1313, 2017.

[5] A. Kulmala, M. Alonso, S. Repo et al., "Hierarchical and distributed control concept for distribution network congestion management," *IET Generation, Transmission & Distribution*, vol. 11, no. 3, pp. 663–673, 2017.

[6] S. Mohtashami, D. Pudjianto, and G. Strbac, "Strategic distribution network planning with smart grid technologies," *IEEE Transactions on Smart Grid*, vol. 8, no. 6, pp. 2656–2664, 2017.

[7] K. Chen, Y. Zhang, and H. Wang, "Fault-section location of distribution network containing distributed generation based on immune algorithm," *Dianli Xitong Baohu yu Kongzhi/ Power System Protection and Control*, vol. 43, no. 24, pp. 37–62, 2017.

[8] A. A. S. Emhemed and G. M. Burt, "An advanced protection scheme for enabling an LVDC last mile distribution network," *IEEE Transactions on Smart Grid*, vol. 3, no. 3, pp. 2602–2609, 2017.

[9] J. Zhao, J. Wang, Z. Xu, C. Wang, C. Wan, and C. Chen, "Distribution network electric vehicle hosting capacity maximization: a chargeable region optimization model," *IEEE Transactions on Power Systems*, vol. 32, no. 3, pp. 4119–4130, 2017.

[10] G. Xu, Z. Wang, J. Zhou et al., "Rotor loss and thermal analysis of synchronous condenser under single-phase short-circuit fault in the transmission line," in *JIEEE Transactions on Energy Conversion*, 2022.

[11] M. Abdelaziz, "Distribution network reconfiguration using a genetic algorithm with varying population size," *Electric Power Systems Research*, vol. 142, no. JAN., pp. 9–11, 2017.

[12] D. Shelar and S. Amin, "Security assessment of electricity distribution networks under DER node compromises," *IEEE Transactions on Control of Network Systems*, vol. 4, no. 1, pp. 23–36, 2017.

[13] L. Kai, S. Zhong, and F. Zhu, "A NDN IoT content distribution model with network coding enhanced forwarding strategy for 3G," *IEEE Transactions on Industrial Informatics*, vol. 14, no. 99, pp. 2723–2733, 2018.

[14] Z. Ma, Y. Shang, H. Yuan et al., "Holistic performance evaluation framework: power distribution network health index," *Iet Generation Transmission & Distribution*, vol. 11, no. 9, pp. 2184–2193, 2017.

[15] S. Han, D. Kodaira, and S. Han, "An automated impedance estimation method in low-voltage distribution network for coordinated voltage regulation," *IEEE Transactions on Smart Grid*, vol. 7, no. 2, pp. 1012–1020, 2017.

[16] L. Wang, S. Sharkh, and A. Chipperfield, "Optimal decentralized coordination of electric vehicles and renewable generators in a distribution network using A* search," *International Journal of Electrical Power & Energy Systems*, vol. 98, no. JUN., pp. 474–487, 2018.

[17] S. Mishra, D. Das, and S. Paul, "A comprehensive review on power distribution network reconfiguration," *Energy Systems*, vol. 8, no. 2, pp. 227–284, 2017.

[18] W. U. Lizhen, L. Jiang, and X. Hao, "Reactive power optimization of active distribution network based on optimal scenario generation algorithm," *Power System Protection & Control*, vol. 43, no. 13, pp. 132–139, 2017.

[19] D. Zeng, G. Wang, and J. Guo, "Adaptive current protection scheme for distribution network with inverter-interfaced distributed generators," *Automation of Electric Power Systems*, vol. 41, no. 12, pp. 86–92, 2017.

[20] Q. Qi, J. Wu, and C. Long, "Multi-objective operation optimization of an electrical distribution network with soft open point," *Applied Energy*, vol. 208, no. dec. 13, pp. 734–744, 2017.

[21] L. Thurner, A. Scheidler, A. Probst, and M. Braun, "Heuristic optimisation for network restoration and expansion in compliance with the single-contingency policy," *Iet Generation Transmission & Distribution*, vol. 11, no. 17, pp. 4264–4273, 2017.

[22] F. U. Yang, J. Liao, and L. I. Zhenkun, "Day-ahead optimal scheduling and operating of active distribution network considering violation risk," *Proceedings of the CSEE*, vol. 37, no. 21, pp. 6328–6338, 2017.

[23] M. Mikolajkova, C. Haikarainen, and H. Saxen, "Optimization of a natural gas distribution network with potential future extensions," *Energy*, vol. 125, pp. 839–848, 2017.